

Article

Gonad and Germ Cell Development and Maturation Characteristics of the Pot-Bellied Seahorse (*Hippocampus abdominalis*) under Captive Breeding Conditions in Northern China

Yichao Zhang ^{1,2,3} , Siyong Qin ⁴, Qinghua Liu ^{2,3,*}  and Wenqi Wang ^{1,*}

¹ School of Marine Science and Engineering, Qingdao Agricultural University, Qingdao 266000, China; 15293184681@163.com

² CAS and Shandong Province Key Laboratory of Experimental Marine Biology, Institute of Oceanology, Chinese Academy of Sciences, Qingdao 266000, China

³ Laboratory for Marine Biology and Biotechnology, Qingdao National Laboratory for Marine Science and Technology, Qingdao 266000, China

⁴ Rizhao Duobao Aquaculture Co., Ltd., Rizhao 276800, China; toubaoyuye@126.com

* Correspondence: qinghualiu@qdio.ac.cn (Q.L.); wenqi31@163.com (W.W.); Tel.: +86-532-82898716 (Q.L.); +86-18506394370 (W.W.)

Abstract: Ovoviviparity and male pregnancy represent distinctive reproductive strategies in seahorses. However, the detailed process of gonadal development in seahorses, particularly in the pot-bellied seahorse (*Hippocampus abdominalis*), remains largely unknown. In this study, we investigated the complete gonadal development process of the pot-bellied seahorse under captive breeding conditions (18 ± 1 °C). Immediately after birth, primordial germ cells (PGCs) were found within the genital ridge, enclosed by a single layer of somatic cells. Around 7–9 days after birth (DAB), the ovary begins to differentiate. By 30 DAB, two germinal ridges had formed along the edge of the follicular lamina in the ovary. The primary oocytes, resulting from this differentiation process, gradually migrated from the dorsal sides to the mid-ventral area of the ovary, eventually maturing into eggs. In the testis, the primary and secondary spermatocytes appeared at 15 and 30 DAB, respectively, preceding the formation of the testicular lumen (50 DAB). The testis was observed to consist of a single large germinal compartment. Under captive breeding conditions in Northern China, the pot-bellied seahorse demonstrated year-round breeding capability, with each male producing approximately 100–150 larvae. The findings from this study contribute valuable insights into seahorse aquaculture and enhance understanding of the unique reproductive strategy employed by seahorses.

Keywords: *Hippocampus abdominalis*; ovoviviparity; germ cell; gonad development; ovary; testis

Key Contribution: The findings of this study provided information on the development of gonads and germ cells in the *Hippocampus abdominalis*, spanning from larvae to adults, found the ovaries of seahorses exhibited a unique two germinal ridge structure. They observed that the testis consisted of a single large germinal compartment in the absence of spermatocyte structures.



Citation: Zhang, Y.; Qin, S.; Liu, Q.; Wang, W. Gonad and Germ Cell Development and Maturation Characteristics of the Pot-Bellied Seahorse (*Hippocampus abdominalis*) under Captive Breeding Conditions in Northern China. *Fishes* **2023**, *8*, 551. <https://doi.org/10.3390/fishes8110551>

Academic Editor: Juan F. Asturiano

Received: 11 October 2023

Revised: 6 November 2023

Accepted: 6 November 2023

Published: 15 November 2023



Copyright: © 2023 by the authors. Licensee MDPI, Basel, Switzerland. This article is an open access article distributed under the terms and conditions of the Creative Commons Attribution (CC BY) license (<https://creativecommons.org/licenses/by/4.0/>).

1. Introduction

Fish reproduction is pivotal in both individual reproductive processes and aquaculture [1]. Further comprehension of gametogenesis and gonadal development is essential for gaining insights into fish reproduction [2,3]. In aquaculture, the quality of gametes determines the success of artificial breeding, with the production of high-quality eggs and seedlings being a primary objective to enhance industry efficiency [4]. Spermatogenesis and oogenesis are intricate processes that play a vital role in transmitting genetic information to the next generation [5]. The origin, development, and maturation of germ cells are subject

to complex and precise regulation, involving both extrinsic (such as hormones and growth factors) and intrinsic (cell-autonomous) regulation [3].

The reproductive strategy is a crucial aspect of an organism's life, profoundly influencing fitness and survival [2]. Fish employ diverse reproductive strategies, including oviparity, where eggs are laid in the water prior to fertilization; viviparity, where embryos develop inside the parental reproductive system and receive direct nutrition [6]; and the recently explored ovoviviparity, where embryos develop internally within parental reproduction organs and receive nutrition from the yolk sac [7,8]. Syngnathid fishes, such as seahorses and pipefish, represent a unique reproduction strategy of ovoviviparity and male pregnancy within the family of approximately 300 species [9,10]. In this extraordinary process, females release mature eggs into the male's brood pouch, where fertilization occurs, followed by the completion of embryonic development. Seahorses possess particularly specific gonadal structures and intricate brood pouch structures [10–12].

Seahorses are widely recognized for their male-ovoviviparous reproduction strategy, where both fertilization and embryo development occur within the male's brood pouch [13]. Research on the seahorse trade, which began in the mid-1990s, revealed that certain species and populations had already suffered from overexploitation [14,15]. The combined effects of overexploitation, incidental bycatch, and habitat loss have led to a drastic decline in the seahorse population worldwide [16,17]. Consequently, in November 2002, all seahorse species were listed under the Convention on International Trade in Endangered Species (CITES) [18]. Currently, there are 46 taxonomically recognized species of seahorses, all belonging to a single genus [19,20]. Due to their unique reproductive strategy and specific breeding environment requirements, only 13 species have been successfully bred in artificial settings [21]. The seahorse exhibits distinctive gonadal structures in addition to its unique brood pouch. Selman et al. (1991) pioneered the study of *Hippocampus erectus* ovarian structure, revealing its distinction from typical bony fishes [11]. *Hippocampus erectus* was the first to examine the ovary structure of its species, revealing differences from most bony fishes. Our investigation revealed that *Hippocampus abdominalis* exhibited a distinct ovarian structure from typical bony fishes, featuring two germinal ridges and an orderly germ cell arrangement. Biagi et al. (2016) identified a unique testis structure in *Hippocampus guttulatus* in contrast to other bony fishes. In cross-section, the testis exhibits a cystic structure with a central lumen, where the initial spermatogenesis occurs. Spermatogenesis occurs in two stages, with the first stage in the spermatocysts and the second stage in the central lumen [12]. While previous studies have primarily focused on seahorse evolution [22–24], environment toxicity [25,26], and brood pouch development [27–32], there remains a limited understanding of sex differentiation, gametogenesis, and gonadal development in seahorses [13,33–35].

Hippocampus abdominalis is a temperate-water species known to grow to heights exceeding 30 cm and weigh up to 30 g [36]. It primarily inhabits shallow water in Australia and New Zealand [20]. In 2016, this species was introduced to China from Australia, and significant advancements in artificial breeding were accomplished by 2020 [1]. In this study, we comprehensively investigate the development of gonads and germ cells in *H. abdominalis*, from larvae to mature adults, under large-scale captive breeding conditions in Northern China. Our investigation includes the localization of primordial germ cells (PGCs), the process of sexual differentiation, and gametogenesis.

2. Materials and Methods

2.1. Animals and Sample Collection

The larvae, juveniles, and adults of *H. abdominalis* used in this study were obtained from Duobao Aquaculture Co., Ltd., located in Rizhao, Shandong Province, China. The seahorses were reared in concrete tanks measuring 25 m × 25 m × 1 m from the larval stage to adulthood. To maintain optimal conditions, the tanks were maintained at a salinity of 2.5‰, a light intensity of 2800 ± 500 lux, and a photoperiod of 15 h of light and 9 h of darkness. The water temperature was controlled at 18 ± 1 °C. Seahorse juveniles were

initially fed with *Artemia nauplii* until they reached two months of age. Juveniles from two months of age to three months of age were fed with frozen *Copepods*. After three months, the adults were fed frozen *Mysidacea*.

Nine larvae were randomly sampled every three days until 30 days after birth (DAB), and successively, six seahorses were sampled biweekly until 165 DAB. To facilitate sampling, the seahorses were individually anesthetized using ethyl-3-aminobenzoate methane sulfonate (MS-222) to ensure they were unconscious before being euthanized for sampling.

2.2. Histology Analysis

The larvae and gonadal tissue obtained from juveniles and adults were fixed in Bouin's solution for 48 h. Subsequently, the samples underwent a series of procedures, including dehydration using an ethanol gradient and treatment with transparent xylene. They were embedded in paraffin. Thin slices with a thickness of 3 μm were obtained using a microtome (Leica Microsystems, Wetzlar, Germany) and stained with hematoxylin and eosin (HE). To visualize the basement membrane, a reticulin staining method was applied [37]. Fix the tissue in a 10% formalin fixative, then conventionally dehydrate and embed. Cut into a paraffin section 3 μm thick and dewax with distilled water. Put the section on the dyeing frame, drop in Gomori Oxidant, and oxidize for 5 min followed by washing with water slightly. Bleach in Oxalic Acid solution for 1–2 min, then rinse in running water for 2 min and slightly with distilled water. Mordant dyeing with Ferric Ammonium Sulfate solution for 5 min and wash lightly with tap water and distilled water. Following mordant dyeing, Gomori Ammoniacal Silver solution was added, and the section was dyed for 3 min. After this step, it was gently washed with distilled water. The section was subsequently reduced using Gomori Reductant for 1 min and thoroughly rinsed in running water for 10 min. Finally, the tissue was conventionally dehydrated and rendered transparent before being sealed with resinene. The prepared slices were sealed with neutral gum and examined using a light microscope with a camera (DS-Ri2; Nikon, Tokyo, Japan). Images were captured for further analysis.

2.3. Immunofluorescence

Testes and ovaries were fixed in 4% (*w/v*) paraformaldehyde (PFA) for 24 h. Following that, the samples underwent dehydration using an ethanol gradient (70%, 80%, 90%, and 100%) and treatment with transparent xylene. They were then embedded in paraffin wax. Subsequently, the samples were transected at a thickness of 4–6 μm using a Leica Microsystems instrument from Germany, Wetzlar (104). After dewaxing and dehydration, the sections were further rehydrated in PBST (Phosphate-buffered saline with Tween-20) for 3 cycles of 5 min each. To block nonspecific binding, the sections were incubated in 4% normal goat serum for 30 min, followed by overnight incubation at 4 °C with an anti-vasa anti-rabbit immunoglobulin G (IgG) (1:400; 128306; Gene Tex, Irvine, CA, USA). The residual antibodies were washed in PBS (Phosphate-buffered saline) for 3 cycles of 10 min each. Subsequently, the sections were incubated with tetramethyl rhodamine isothiocyanate (TRITC)-conjugated goat anti-rabbit immunoglobulin G (IgG) (H + L) (1:300; Bio Basic Inc., Amherst, NY, USA) and 6-diamidino-2-phenylindole (DAPI, 1 $\mu\text{g}/\text{mL}$ diluted in PBS) for 1 h at room temperature. Images were captured using a laser microscope (DS-Ri2; Nikon, Japan, Tokyo).

2.4. Statistical Analysis

The statistical analysis was performed using SPSS version 20.0 software (SPSS Inc., Chicago, IL, USA). The data were presented as the mean \pm SD (standard deviation). To compare the sex ratio of *Hippocampus abdominalis*, a chi-square test was employed.

3. Results

3.1. Growth

Figure 1 depicts the total length (TL) of the *Hippocampus abdominalis* at various life stages, including larvae, juveniles, and adults. The TL growth curve displays a reverse S-shape, with a period of slow growth observed 30 days after birth (DAB). Subsequently, there is a notable period of slowed growth occurring between 55 and 90 DAB. Nevertheless, after reaching 90 DAB, juveniles undergo a phase of rapid growth.

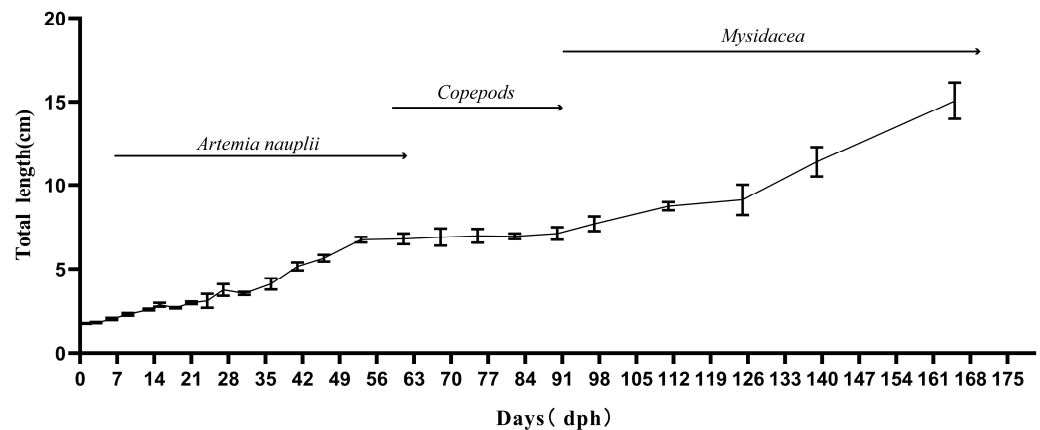


Figure 1. The total length of the breeding group of pot-bellied seahorses is from 0 to 165 DAB. Roughly 10 individuals were sampled at each stage. The curve of total length is reverse S-shaped, showing periods of retarded growth from 55 to 90 DAB and rapid growth from 90 to 165 DAB.

3.2. The Gonadal Primordium and Ovarian Differentiation of *H. abdominalis*

Gonadal primordium was first detected at 0 days after birth (DAB), situated beneath the notochord. Inside the gonadal primordium (Figure 2(A1,A2)), both primordial germ cells (PGCs) and somatic cells were ensconced by somatic epithelial cells. PGCs were distinguishable from somatic cells by their markedly larger size (diameter: $9.2 \pm 0.81 \mu\text{m}$), elliptical shape, and the presence of a prominent nucleus with a distinct nucleolus (Figure 2(A1,A2)) [4].

Ovarian differentiation was initially observed at 7 DAB. A distinct cavity was found within a specific area of the gonads, classifying them as ovaries. Gonads lacking this cavity were classified as testes. The testis displayed a flat cross-sectional shape primarily composed of spermatogonia. At the same developmental stage, the testes were notably smaller than the ovaries. The biological sex of 32 larvae and juveniles was randomly tested. The count of female seahorses was 18, while male seahorses numbered 16, resulting in a 1:1 biological sex ratio of *H. abdominalis* ($p = 0.616 > 0.05$) compared to the theoretical expectation.

3.3. Ovarian Developmental Characteristics of *H. abdominalis*

At 10 DAB, the ovaries displayed an elliptical cross-sectional shape. Within the ovary, primary oocytes at the chromatin nucleolus stage were detected. By 30 DAB, oocytes in the perinucleolous phase could be observed within the ovary (Figure 3(B1)). Two distinct germinal ridges (GR) initially emerged on either side of the ovarian cavity (Figure 3(B1,B2)). At 50 DAB, oocytes had advanced to stage II, with primary oocytes remaining the predominant type in the ovaries (Figure 3(C1)). The follicular lamina, bounded externally by the ovarian wall and internally by the luminal epithelium, was visible. All germ cells originated from the GR located at the end of the ovary and were arranged sequentially. They developed and gradually moved toward the middle of the ovary (Figure 3(C1)).

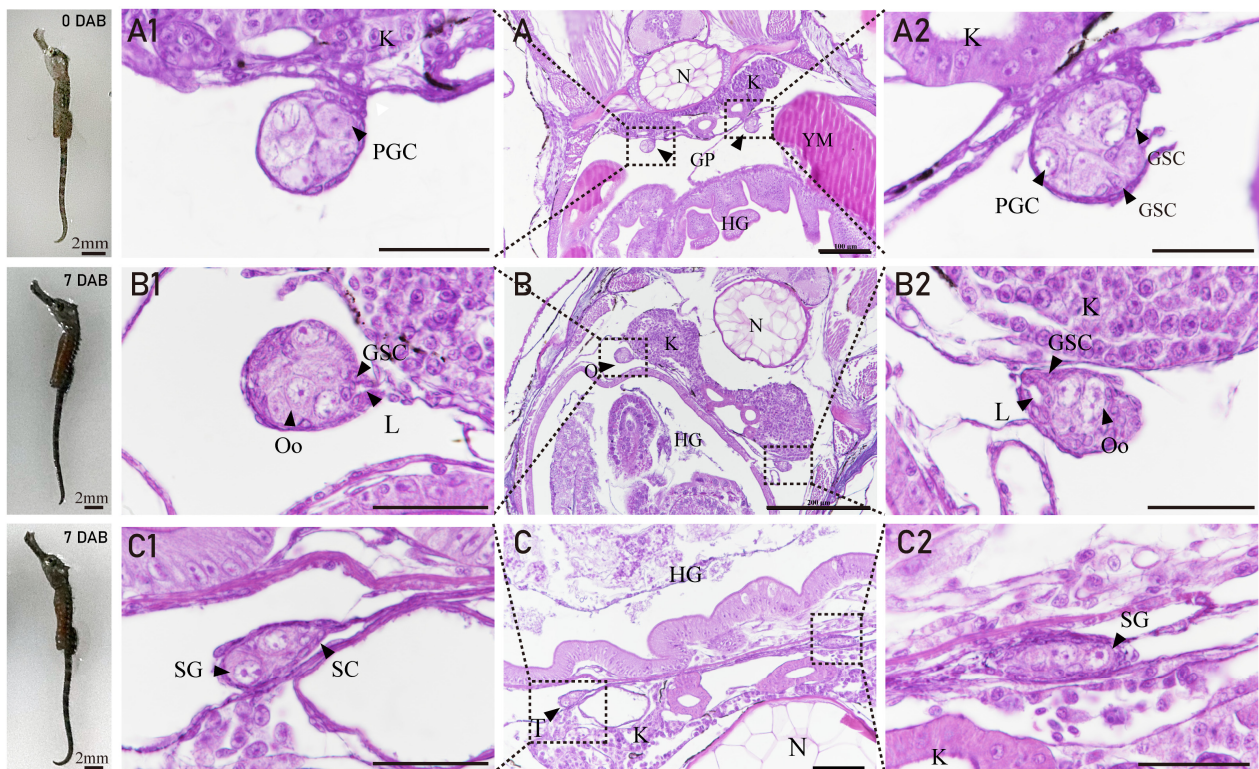


Figure 2. The gonadal primordium and gonad differentiation. (A) Primordial germ cells completed migration at 0 DAB; (A1,A2) Magnified image in panel (A); (B) at 7 DAB, ovary lumen was observed in gonads; (B1,B2) magnified image in panel (B); (C) at 7 DAB, without the presence of this cavity, it was observed in the testis; (C1,C2) magnified image in panel (C). GP: gonadal primordium; YS: yolk mass; K: kidney; PGCs: primordial germ cells; N: notochord; HG: hindgut; O: ovary; Oo: oogonia; SC: Sertoli cells; L: ovary lumen; SG: spermatogonia; T: testis; GSC: gonadal somatic cells; PF: perfoliate cell. Scale bars: 200 μm (B); 100 μm (A); 50 μm (C); 25 μm (A1,A2,B1,B2,C1,C2).

At 100 DAB, the ovaries exhibited a slightly transparent, elongated columnar shape with an orange–yellow hue. Over half of the ovarian volume was primarily filled with oocytes in the cortical alveolus stage and oil droplet stage (Figure 3(D1)). The oocytes were surrounded by a layer of follicular cells (Figure 3(D2)). Additionally, the zona radiata, located between the follicular layer and the plasma membrane, became visible (Figure 3(D2)).

At 120 DAB, the ovary displayed an orange–yellow color attributed to the presence of vitellogenin (Figure 4(A1)). The oocyte layer comprised oocytes at multiple stages, encompassing the chromatin nucleolar stage, perinucleolar stage, cortical alveolus stage, early vitellogenic stage, and late vitellogenic stage (Figure 4(A1)). During the early vitellogenic stage, the yolk granules were arranged peripherally in the cytoplasm (Figure 4(A1)). The surrounding follicular cells showed clear differentiation into cubic granulosa cells in the inner layer and theca cells. However, the structure of theca cells was not clear in the observations (Figure 4(A2)). During the late vitellogenic stage, oocytes exhibited augmented cellular volume, accompanied by a conspicuous rise in both yolk granule quantity and size within the cytoplasm (Figure 4(A2)).

At 150 days after birth (DAB), the ovaries of adult fish had achieved full maturity, reached their maximum volume, and occupied roughly half of the abdominal cavity. During this stage, the oocyte underwent nuclear envelope disappearance and cell depolarization, resulting in a significant increase in size due to hydration. The oocytes became translucent due to the disassembly of crystalline yolk proteins (Figure 4(C1)). Mature eggs nearly entirely occupied the entire ovarian cavity (Figure 4(C1,C2)).

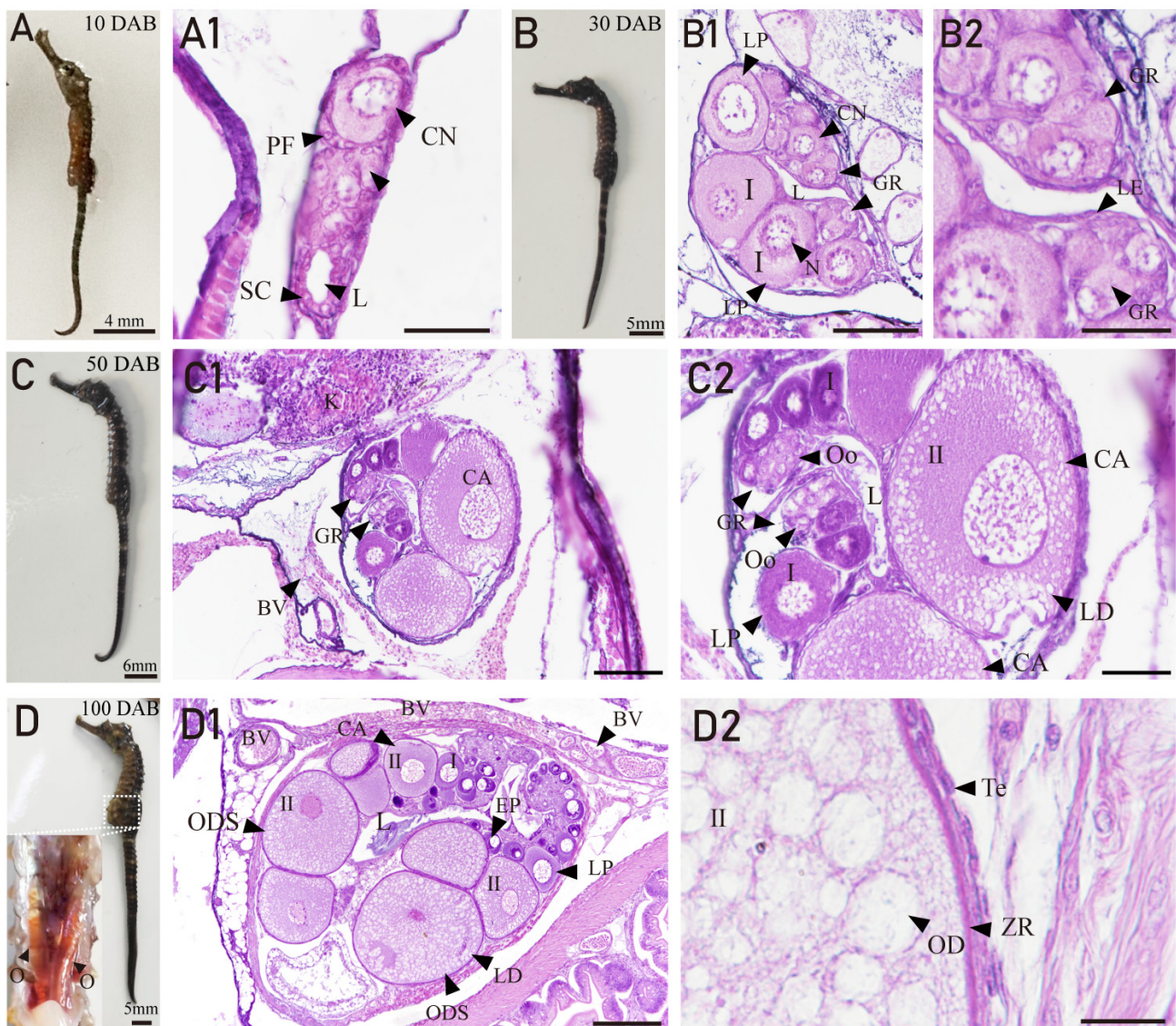


Figure 3. The formation of two germinal ridges and primary oocyte development. (A–D) Illustration of female seahorses at 10 DAB, 30 DAB, 50 DAB, and 100 DAB; (A1) at 10 DAB, the primary oocytes began to appear in the gonad; (B1) at 30 DAB, the size of primary oocytes increased, and two germinal ridges formed. At the same time, prefollicle cells and the cortical alveolus stage appeared; (B2) magnified image in panel (B1); (C1) at 50 DAB, the cortical alveolus stage oocytes began to appear in the gonad; (C2) magnified image in panel (C1); (D1) at 100 DAB, oocytes entered the oil droplet stage and the follicular layer differentiated into two layers; (D2) oil droplet stage oocytes. GR: germinal ridge; PGCs: primordial germ cells; SC: somatic cells; PF: prefollicle cells; CN: chromatin nucleolar stage; LE: luminal epithelium; L: ovary lumen; LP: late perinucleous stages; N: nucleolus; Oo: oogonia; PO: primary oocytes; BV: blood vessels; EP: early perinucleolus stage; FC: follicle cells; GR: germinal ridge CA: cortical alveolus stage; OD: oil droplet; ODS: oil droplet stage; YM: yolk mass; LD: lipid droplet; LV: late vitellogenic stage; EV: early perinucleolus stage; Te: theca cells; ZR: zona radiata; YG: yolk granules. Scale bars: 200 μm (D1); 100 μm (C1); 50 μm (C2,B1); 25 μm (A1,D2); 20 μm (B2).

3.4. Developmental Characteristics of the Testis in *H. abdominalis*

At 15 DAB, the germinal epithelium consisted of Sertoli cells and germ cells, supported by the basement membrane (Figure 5(A1,A2)). Within the germinal compartment, two types of germ cells were identified: spermatogonia and primary spermatocytes. The spermatogonia cells were measured to be $9.59 \pm 0.72 \mu\text{m}$ in size, with a cell nucleus diameter of $5.22 \pm 0.28 \mu\text{m}$ (Figure 5(A1)). Primary spermatocytes were distinguished

by an unclear boundary around their nucleus, and the chromosomes appeared loosely arranged (Figure 5(A1)).

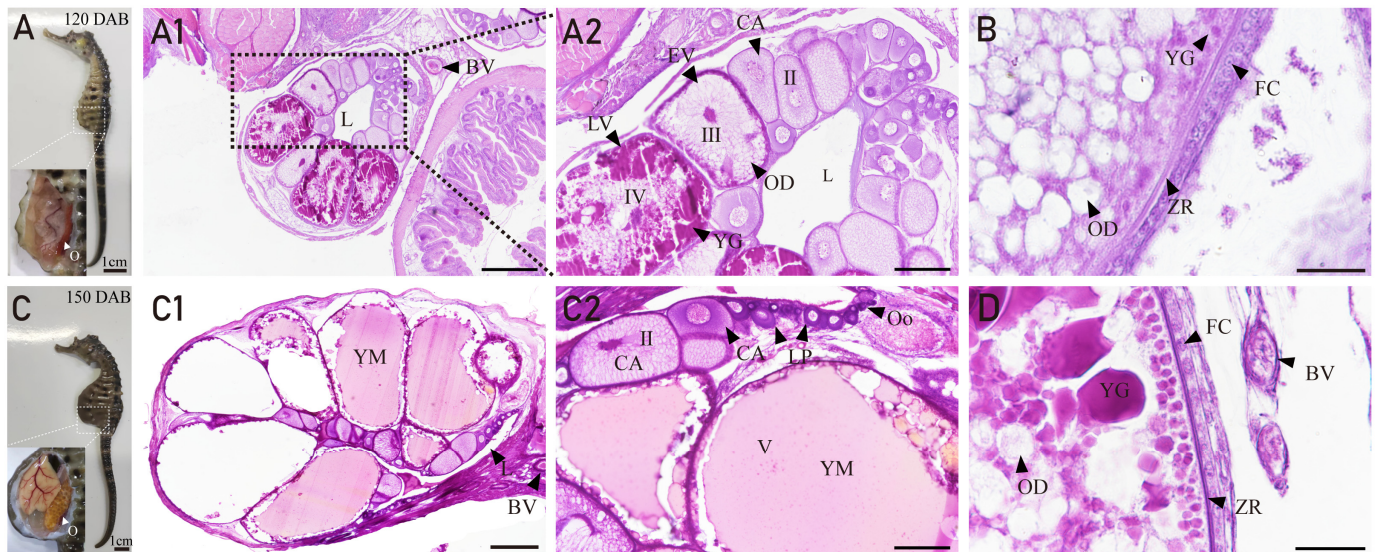


Figure 4. The process of ovary and oocyte maturation from 120 to 150 DAB. (A) Illustration of a female seahorse at 120 DAB; (A1) at 120 DAB, oocytes entered the vitellogenic stage; (A2) magnified image in panel (A1); (B) the follicle layer of early vitellogenic stage oocytes; (C) illustration of a female seahorse at 150 DAB; (C1) at 150 DAB, the ovary reached full maturity; (C2) magnified image in panel (C1); (D) the follicle layer of late vitellogenic stage; L: ovary lumen; LP: late perinucleolus stages; N: nucleolus; BV: blood vessels; FC: follicle cells; GR: germinal ridge; CA: cortical alveolus stage; OD: oil droplet; ODS: oil droplet stage; YM: yolk mass; LD: lipid droplet; LV: late vitellogenic stage; EV: early perinucleolus stage; ZR: zona radiata; YG: yolk granules. Scale bars: 500 μm (A1,C1); 200 μm (A2,C2); 25 μm (B,D).

At 30 DAB, secondary spermatocytes were initially detected in the testes (Figure 5(B2)). The diameter of secondary spermatocytes ($6.93 \pm 1.41 \mu\text{m}$) and the size of their nuclei continued to decrease, accompanied by a reduction in the cytoplasm. At 50 DAB, the presence of a central lumen was first observed in the middle of the testis (Figure 5(C2)). By 100 DAB, the germinal epithelium displayed a wave-like pattern owing to the asynchronous and rapid proliferation and differentiation of germ cells. The arrangement of germ cells from outer to inner layers included spermatogonia, primary spermatocytes, secondary spermatocytes, and spermatids (Figure 5(D2)). Numerous secondary spermatocytes migrated towards the border of the germinal epithelium (Figure 5(D1,D2)). A small number of spermatids were found within the central lumen, surrounded by flocculent substances occupying the center of the central lumen (Figure 5(D1)).

At 120 DAB, there was a significant increase in the number of secondary spermatocytes within the central lumen (Figure 6(A1)). By 150 DAB, the testes had reached full maturity, with the presence of spermatozoa within the central lumen (Figure 6(B1)). The testis appears as a column shape with a large central lumen and a thin wall (Figure 6(B1)). The wall consisted of the tunica albuginea and germinal epithelium (Figure 6(B2)). Spermatogonia were distributed throughout the germinal epithelium (Figure 6(B2)). Nevertheless, the structure of the spermatocysts was not distinctly visible in tissue sections (Figure 6(C)). This type of spermatogenesis belongs to semicyclic spermatogenesis.

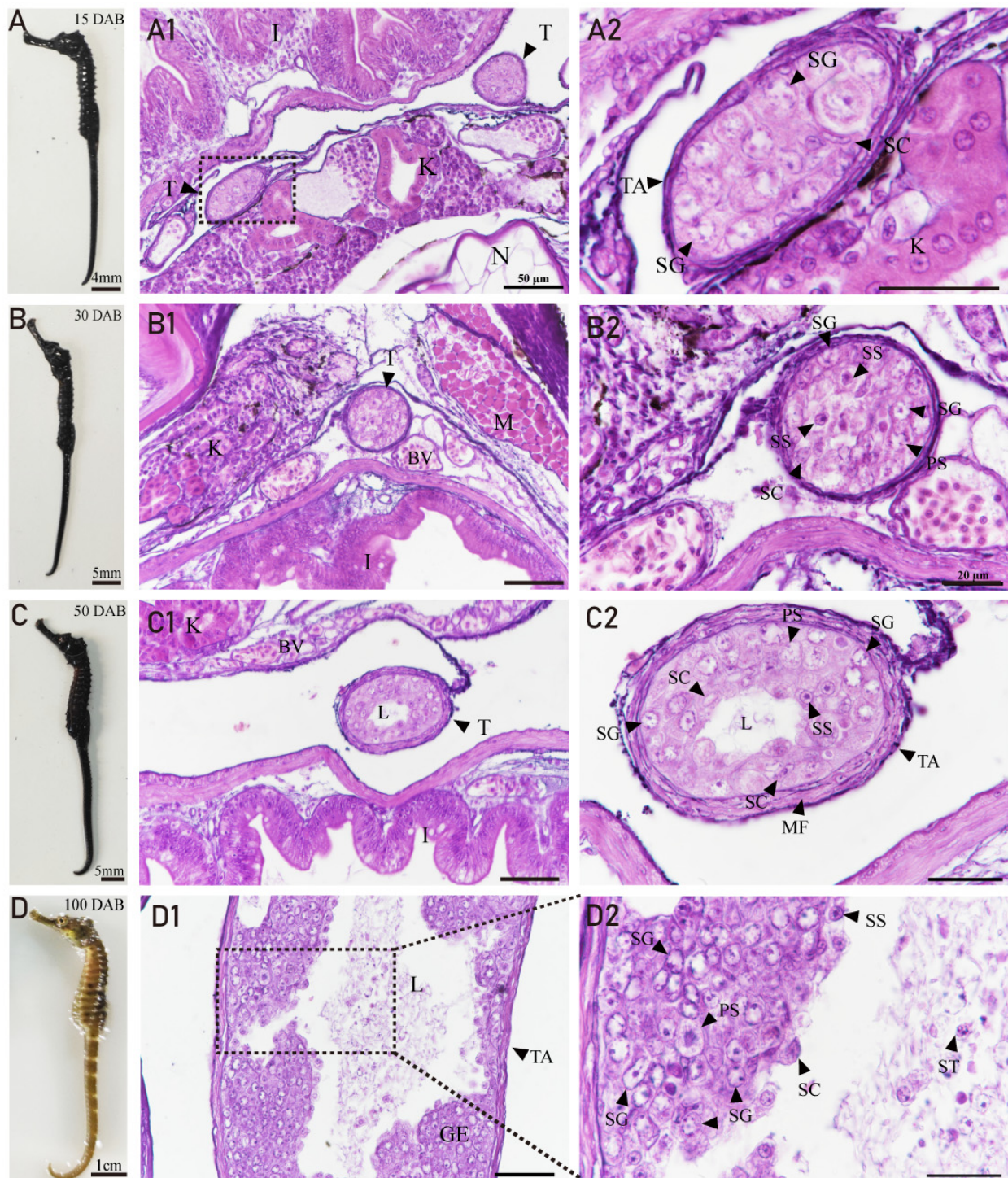


Figure 5. The development of testis from 15 to 100 DAB. (A–D) Illustration of male seahorses at 15 DAB, 30 DAB, 50 DAB, 100 DAB; (A1) at 15 DAB, primary spermatocytes appeared in the testes; (A2) magnified image in panel (A1); (B1) at 30 DAB, secondary spermatocytes appeared in the testes; (B2) magnified image in panel (B1); (C1) at 50 DAB, the central lumen formed in the testes; (C2) magnified image in panel (C1); and (D1) at 100 DAB, the spermatids began to appear in the central lumen; (D2) magnified image in panel (D1). I: intestine; N: notochord; K: kidney; T: testes; SC: Sertoli cells; TA: tunica albuginea; SG: spermatogonia; SS: secondary spermatocytes; MF: muscle fibers; PS: primary spermatocytes; L: central lumen; GE: germinal epithelium; ST: spermatids. Scale bars: 50 μ m (A1–D1); 25 μ m (A2,B2,C2,D2).

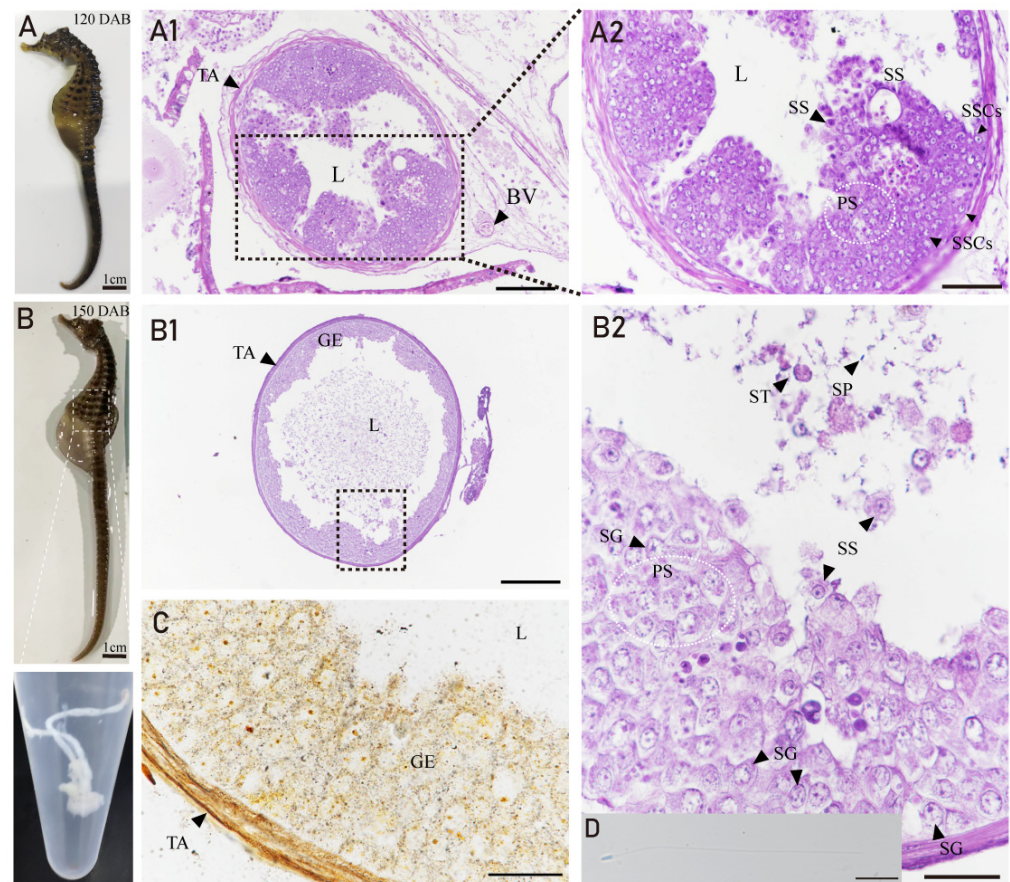


Figure 6. Testis development and sperm maturation. (A–B) Illustration of male seahorses at 120 DAB, and 150 DAB; (A1) at 120 DAB, the number of spermatids increased; (A2) magnified image in panel (A1); (B1) at 150 DAB, the structure of mature testis; (B2) magnified image in panel (B1); (C) the basement membrane was enhanced by the reticulin method; (D) the optical microstructure of the spermatozoa of *H. abdominalis* TA: tunica albuginea; L: central lumen; BV: blood vessel; SG: spermatogonia; SS: secondary spermatocytes; GE: germinal epithelium; ST: spermatids; SP: spermatozoa; PS: primary spermatocytes. Scale bars: 500 μm (B1); 100 μm (A1); 50 μm (A2); 25 μm (B2,C); 10 μm (D).

3.5. Expression of *Vasa* in Gonads of *H. abdominalis* by Immunofluorescence

The localization of PGCs in gonads was investigated using tissue section immunofluorescence with anti-vasa antibodies. At 0 DAB and 6 DAB, strong vasa expression was observed in PGCs of the gonadal primordium (Figure 7(A1,A3,B1,B3)). By 10 DAB, vasa signals were detected in the cytoplasm of spermatogonia, oogonia, and primary oocytes (Figure 7(C3,D3)). At 150 DAB, vasa signals were predominantly found in spermatogonia and primary spermatocytes, with few signals in spermatids (Figure 7(E3)). At 150 DAB, the vasa signal was evenly distributed in the cytoplasm of oogonia (stage I) and primary oocytes (stage II). At the cortical alveoli stage, the vasa signals appeared as numerous small particles primarily located in the peripheral region of the cytoplasm (Figure 7(F3)). During the early vitellogenic stage, the vasa signals decreased significantly and were distributed in the cytoplasm (Figure 7(F3)). At a late vitellogenic stage, as vitellogenesis progressed, the vasa signal became difficult to discern, possibly due to the dispersion of vasa protein into the enlarged oocytes (Figure 7(F3)).

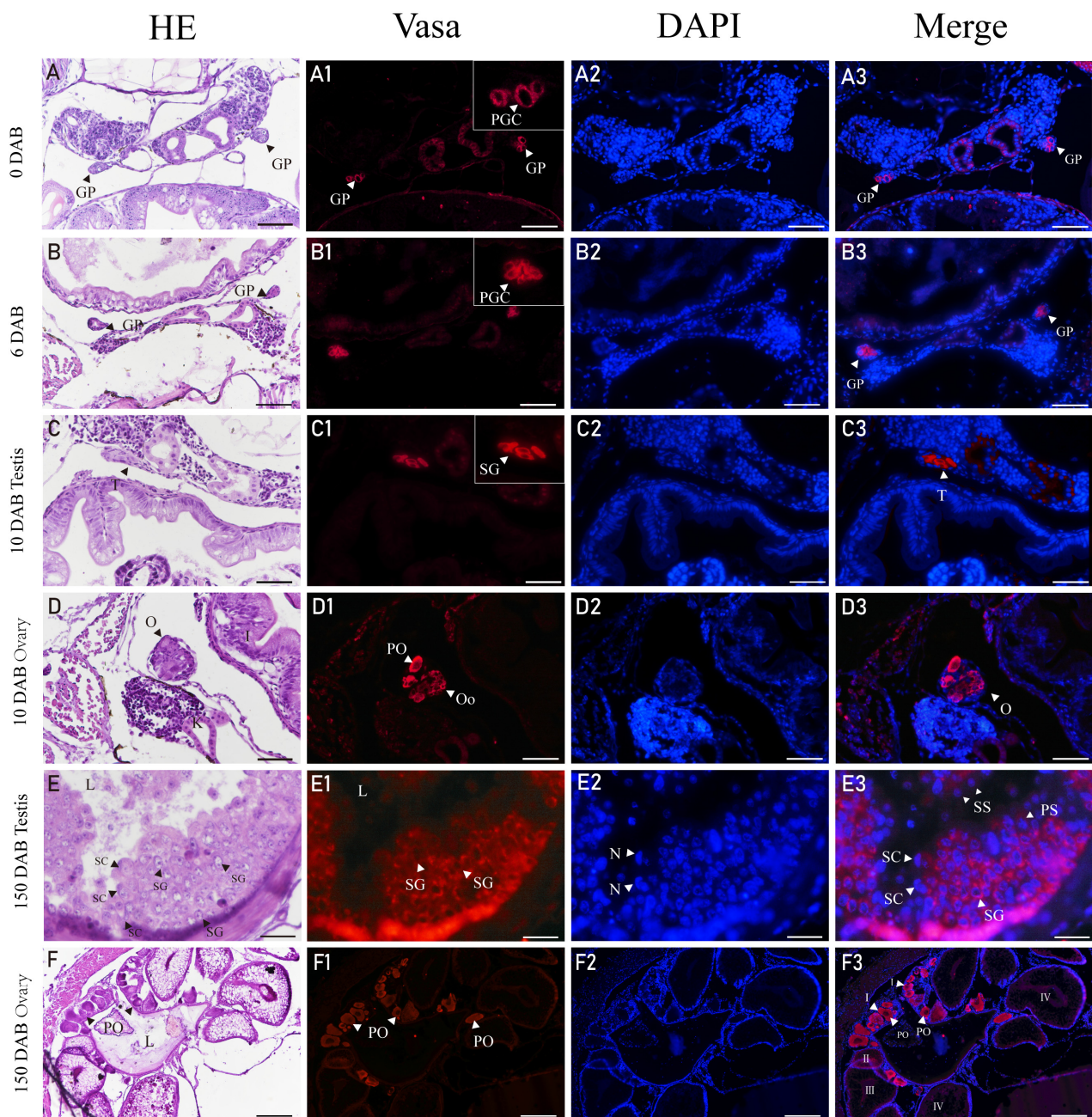


Figure 7. Distribution of vasa signals in different development stages of the ovary and testis. (A1) Immunofluorescence of the vasa in gonadal primordium at 0 DAB. (B1) Immunofluorescence of the vasa in gonads at 6 DAB vasa are expressed in the cytoplasm of germ cells. (C1) Immunofluorescence of vasa in the testes of 10 DAB males. (D1) Immunofluorescence of vasa in the ovaries of 10 DAB females. (E1) Immunofluorescence of vasa in the testes of 150 DAB males. (F1) Immunofluorescence of the vasa in the ovaries of 150 DAB females. (A2–F2) Nuclei of the testis and ovarian section were stained by DAPI (blue). (A3–F3) Vasa and nucleus are shown in red and blue, respectively. The vasa and nucleus are shown in red and blue, respectively. GP: gonadal primordium; PGCs: primordial germ cell; T: testis; O: ovary; PO: primary growth oocytes; SG: spermatogonia; SC: Sertoli cells; SS: secondary spermatocytes; PS: primary spermatocytes; K: kidney; I: intestine. Scale bars: 200 μm ((F), F1–F3); 50 μm ((A), A1–A3, (B), B1–B3, (C), C1–C3, (D), D1–D3); 25 μm ((E), E1–E3).

4. Discussion

In this study, we investigated the development of gonads and germ cells in *H. abdominalis* from PGCs to mature eggs and spermatozoa under captive breeding conditions. At

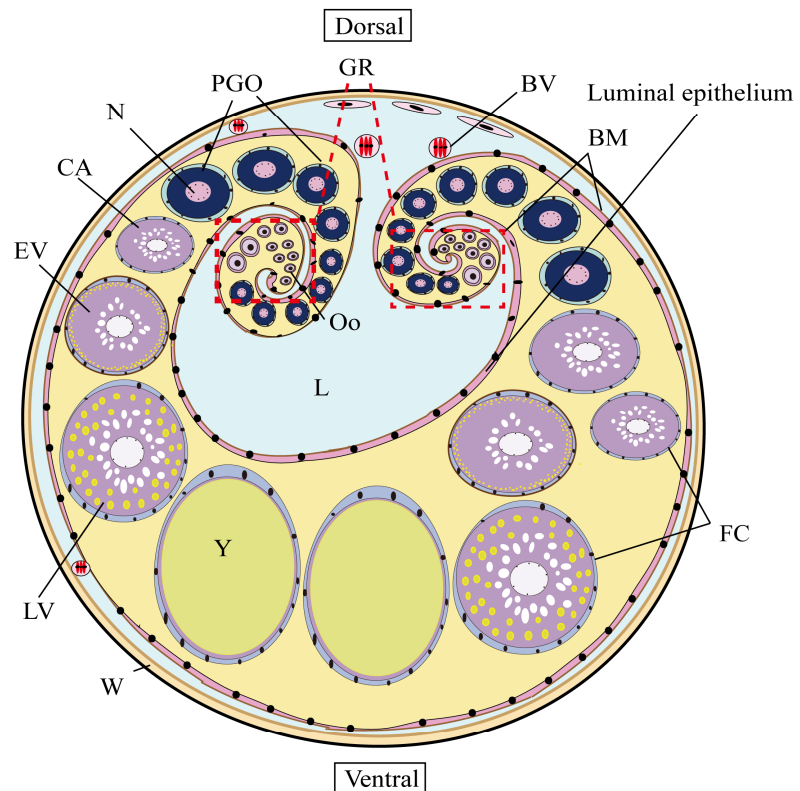
0 DAB, PGCs migrated to the genital ridge and became enclosed by somatic cells under the notochord. In various species, such as *Seriola lalandi*, histological observations combined with the analysis of the PGC migration factor SDF1 have shown that PGCs typically reach the location of the gonadal primordium around 15–20 days after hatching. Days 1–22 are recognized as critical time points for PGC migration [38]. In contrast, *Ctenogobius giurinus* did not form gonadal progenitor bases until 8 days post-hatching, whereas *Scophthalmus maximus* exhibited this formation 15 days after hatching [39,40]. The presence of strong immunofluorescence signals in the vasa confirmed the presence of PGCs within the gonadal primordium. In teleosts, initial ovarian differentiation is commonly characterized by the occurrence of meiotic germ cells or the formation of the ovarian cavity [1,41,42]. In the case of *H. abdominalis*, the formation of the ovarian lumen was observed at 7 DAB, and oogonia entered meiosis at 9 DAB. This finding suggests that somatic cell differentiation precedes the differentiation of germinal cells in this species. Similar observations of the emergence of chromatin nucleolar stage oocytes have been reported in *H. guttulatus* and *H. reidi* at 15 days post-hatching (dph) and 12 dph, respectively [18,43].

Another unique feature of seahorses is the presence of two germinal ridges in the ovary. At 30 DAB, transverse sections of the ovary revealed the presence of two germinal ridges located along the edge of the follicular lamina (Figure 8). These germinal ridges acted as the primary source of germ stem cells, continually generating germ cells. Subsequently, the oocyte departs from the germinal ridge and undergoes maturation. These findings align with previous research regarding gonadal structures in seahorses. In contrast to other teleosts, such as *Paralichthys olivaceus* and *Sebastes schlegelii*, which lack a consistent double germinal ridge structure. Each female seahorse can lay 100–150 eggs approximately every 23 days, which aligns with the developmental period of embryos in the male brood pouch.

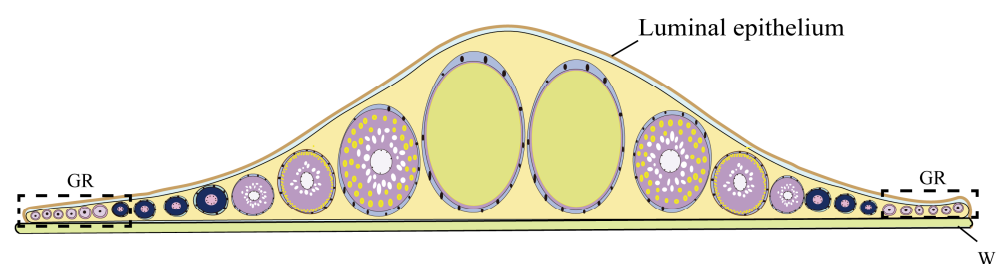
Regarding the testes at 15 DAB, the initiation of meiosis led to the appearance of primary spermatocytes, signifying testicular differentiation. Secondary spermatocytes were observed at 30 DAB, and the formation of the testicular lumen occurred at 50 DAB. The testes exhibited a characteristic structure with a single central lumen surrounded by the tunica albuginea and the germinal epithelium. Notably, in this study, the emergence of secondary spermatocytes preceded the formation of the central lumen in the testes, which differs from the pattern observed in most other teleost species, where the development of the lobular lumen and sperm duct typically precedes the meiosis of spermatogonia [42,44,45].

In *H. abdominalis*, the development of spermatids progresses to spermatozoa within the central lumen at 150 DAB. The germinal epithelium displays a wave-like pattern resulting from variations in the speed of germ cell proliferation and differentiation across distinct regions. Once the primary spermatocytes develop into secondary spermatocytes, they move towards the fringe of the germinal epithelium and eventually enter the central lumen, where they undergo maturation into spermatozoa. This type of spermatogenesis is termed “semicyclic spermatogenesis”, where spermatocytes or spermatids are released into the lumen and mature into spermatozoa [12]. This characteristic aligns with previous studies in syngnathid fish [46–49]. In addition, no distinct spermatocyst structures, which are typical in other teleost species, were observed in *H. abdominalis*, even with intensified staining using the reticulin method. This structure of the testis differs significantly from previous studies on the testicular structure of teleostei. For instance, in the developing testes of *Cyprinus carpio*, germ cell proliferation leads to the formation of spherical cell clusters. Within these clusters, each spermatogonium is surrounded by one or more pre-Sertoli cells, resulting in the formation of cysts. The acinar clusters of spermatogonia that are scattered throughout the gonad also become partially surrounded by the basement membrane [50]. Similar observations of the absence of spermatocyst structures have also been reported in *Syngnathus schlegelii* [51]. These characteristics in *H. abdominalis* differ from those of *H. guttulatus* and *Syngnathus abaster*, where the germinal epithelium is composed of numerous typical spermatocysts [12,47]. This type of spermatogenesis and the absence of spermatocysts could lead to a reduced number of simultaneously mature sperm, and it has been interpreted as one of the possible mechanisms evolved to reduce the cost of

sperm production [52]. Because of their low fecundity and absence of sperm competition in seahorses, they do not have to spend more energy on sperm production [48,53]. The findings of this study provided a theoretical foundation for investigating the adaptive evolution of reproductive strategies in marine organisms. Additionally, they offer a biological underpinning for further delving into the molecular regulation mechanisms governing gonad development in seahorses.



(A) Ovarian cross section



(B) Unrolled ovarian cross section

Figure 8. A schematic representation illustrating ovarian structure. (A) Ovarian cross-section. (B) The ovary has been cut along its dorsal midline, and both halves have been unrolled. CA: oocytes at the cortical alveolus stage; LV: oocytes at the late vitellogenic stage; EV: oocytes at the early vitellogenic stage; FC: follicle cells; W: ovarian wall; Y: yolk sphere; SC: somatic cells; N: nucleolus; BM: basement membrane; BV: bleed vessel; L: ovary lumen; PGO: primary oocytes; Oo: oogonia; GR: germinal ridges.

5. Conclusions

This study demonstrated the characteristics of growth and sexual differentiation, gonad development, and gametogenesis in *H. abdominalis* under captive breeding conditions. We confirmed the two germinal ridges in the ovary and the semi-cystic pattern with no spermatocyte structures in the testes. This result provides essential foundational data for a deeper understanding of the unique reproductive strategy employed by seahorses.

Author Contributions: Conceptualization, writing—review and editing, Q.L.; experimental, methodology, validation, writing—review and editing, Y.Z.; resources, S.Q. and W.W. All authors have read and agreed to the published version of the manuscript.

Funding: This work was supported by the Research and Development Program of Shandong Province (2021LZGC029), the Shandong Province Natural Science Foundation (ZR2020KC038), and the China Agriculture Research System (CARS-47).

Institutional Review Board Statement: The study was conducted in accordance with the Declaration of Helsinki and approved by the Animal Protection and Utilization Committee of the Institute of Oceanography, Chinese Academy of Sciences (Approval Code: IOCAS20231010PPFA0008; Approval Date: 10 October 2023).

Data Availability Statement: Data are contained within the article.

Conflicts of Interest: I hereby declare that the work described in this paper constitutes original research that has not been previously published and is not currently under consideration for publication elsewhere. Each author has reviewed and approved the content of the submitted manuscript and has given consent to be listed as an author. Furthermore, we affirm that there are no known competing financial interests or personal relationships that could have influenced the findings presented in this paper.

References

1. Strüssmann, C.A.; Nakamura, M. Morphology, endocrinology, and environmental modulation of gonadal sex differentiation in teleost fishes. *Fish Physiol. Biochem.* **2002**, *26*, 13–29. [[CrossRef](#)]
2. Li, J.; Lyu, L.; Wen, H.; Li, Y.; Wang, X.; Zhang, Y.; Yao, Y.; Qi, X. Comparative transcriptomic analysis of gonadal development and renewal in the ovoviparous black rockfish (*Sebastes schlegelii*). *BMC Genom.* **2021**, *22*, 874. [[CrossRef](#)] [[PubMed](#)]
3. Schulz, R.W.; de Franca, L.R.; Lareyre, J.J.; Le Gac, F.; Chiarini-Garcia, H.; Nobrega, R.H.; Miura, T. Spermatogenesis in fish. *Gen. Comp. Endocrinol.* **2010**, *165*, 390–411. [[CrossRef](#)] [[PubMed](#)]
4. Yang, Y.; Liu, Q.; Xiao, Y.; Wang, X.; An, H.; Song, Z.; You, F.; Wang, Y.; Ma, D.; Li, J. Germ Cell Migration, Proliferation and Differentiation during Gonadal Morphogenesis in All-Female Japanese Flounder (*Paralichthys olivaceus*). *Anat. Rec.* **2018**, *301*, 727–741. [[CrossRef](#)]
5. Gong, G.; Xiong, Y.; Xiao, S.; Li, X.Y.; Huang, P.; Liao, Q.; Han, Q.; Lin, Q.; Dan, C.; Zhou, L.; et al. Origin and chromatin remodeling of young X/Y sex chromosomes in catfish with sexual plasticity. *Natl. Sci. Rev.* **2023**, *10*, nwac239. [[CrossRef](#)]
6. Planas, J.V.; Swanson, P. Physiological function of gonadotropins in fish. In *Fish Reproduction*; CRC Press: Boca Raton, FL, USA, 2008; pp. 37–66.
7. Lyu, L.; Wen, H.; Li, Y.; Li, J.; Zhao, J.; Zhang, S.; Song, M.; Wang, X. Deep Transcriptomic Analysis of Black Rockfish (*Sebastes schlegelii*) Provides New Insights on Responses to Acute Temperature Stress. *Sci. Rep.* **2018**, *8*, 9113. [[CrossRef](#)]
8. Mori, H.; Nakagawa, M.; Soyano, K.; Koya, Y. Annual reproductive cycle of black rockfish *Sebastes schlegelii* in captivity. *Fish. Sci.* **2003**, *69*, 910–923. [[CrossRef](#)]
9. Lin, Q.; Fan, S.; Zhang, Y.; Xu, M.; Zhang, H.; Yang, Y.; Lee, A.P.; Woltering, J.M.; Ravi, V.; Gunter, H.M.; et al. The seahorse genome and the evolution of its specialized morphology. *Nature* **2016**, *540*, 395–399. [[CrossRef](#)]
10. Stolting, K.N.; Wilson, A.B. Male pregnancy in seahorses and pipefish: Beyond the mammalian model. *Bioessays* **2007**, *29*, 884–896. [[CrossRef](#)]
11. Selman, K.; Wallace, R.A.; Player, D. Ovary of the seahorse, *Hippocampus erectus*. *J. Morphol.* **1991**, *209*, 285–304. [[CrossRef](#)]
12. Piras, F.; Biagi, F.; Taddei, A.R.; Fausto, A.M.; Farina, V.; Zedda, M.; Floris, A.; Franzoi, P.; Carcupino, M. Male gonads morphology, spermatogenesis and sperm ultrastructure of the seahorse *Hippocampus guttulatus* (Syngnathidae). *Acta Zool.* **2015**, *97*, 325–333. [[CrossRef](#)]
13. Wilson, A.B.; Vincent, A.; Ahnesjö, I.; Meyer, A. Male Pregnancy in Seahorses and Pipefishes (Family Syngnathidae): Rapid Diversification of Paternal Brood Pouch Morphology Inferred from a Molecular Phylogeny. *J. Hered.* **2001**, *92*, 159–166. [[CrossRef](#)] [[PubMed](#)]
14. McPherson, J.M.; Vincent, A.C.J. Assessing East African trade in seahorse species as a basis for conservation under international controls. *Aquat. Conserv. Mar. Freshw. Ecosyst.* **2004**, *14*, 521–538. [[CrossRef](#)]
15. Giles, B.G.; Ky, T.S.; Hoang, D.H.; Vincent, A.C.J. The catch and trade of seahorses in Vietnam. *Biodivers. Conserv.* **2006**, *15*, 2497–2513. [[CrossRef](#)]
16. Rosa, I.L.; Oliveira, T.P.R.; Osório, F.M.; Moraes, L.E.; Castro, A.L.C.; Barros, G.M.L.; Alves, R.R.N. Fisheries and trade of seahorses in Brazil: Historical perspective, current trends, and future directions. *Biodivers. Conserv.* **2011**, *20*, 1951–1971. [[CrossRef](#)]
17. Vincent, A.G.; Vincent, A.C.J.; Vincent, A.; Vincentsalomon, A. *The International Trade in Seahorses*; TRAFFIC International: Cambridge, UK, 1996.
18. Novelli, B.; Socorro, J.A.; Caballero, M.J.; Otero-Ferrer, F.; Segade-Botella, A.; Molina Dominguez, L. Development of seahorse (*Hippocampus reidi*, Ginsburg 1933): Histological and histochemical study. *Fish. Physiol. Biochem.* **2015**, *41*, 1233–1251. [[CrossRef](#)]

19. Kuitert, R.H. A new pygmy seahorse (Pisces: Syngnathidae: Hippocampus) from Lord Howe Island. *Rec. Aust. Mus.* **2003**, *55*, 113–116. [[CrossRef](#)]
20. Lourie, S.A.; Foster, S.J.; Cooper, E.W.T.; Vincent, A.C. A Guide to The Identification of Seahorses. *Proj. Seahorse TRAFFIC N. Am.* **2004**, *114*, 1–120.
21. Koldewey, H.J.; Martin-Smith, K.M. A global review of seahorse aquaculture. *Aquaculture* **2010**, *302*, 131–152. [[CrossRef](#)]
22. Li, C.; Olave, M.; Hou, Y.; Qin, G.; Schneider, R.F.; Gao, Z.; Tu, X.; Wang, X.; Qi, F.; Nater, A.; et al. Genome sequences reveal global dispersal routes and suggest convergent genetic adaptations in seahorse evolution. *Nat. Commun.* **2021**, *12*, 1094. [[CrossRef](#)]
23. Teske, P.R.; Cherry, M.I.; Matthee, C.A. The evolutionary history of seahorses (Syngnathidae: Hippocampus): Molecular data suggest a West Pacific origin and two invasions of the Atlantic Ocean. *Mol. Phylogenet. Evol.* **2004**, *30*, 273–286. [[CrossRef](#)] [[PubMed](#)]
24. Foster, S.; Wiswedel, S.; Vincent, A. Opportunities and challenges for analysis of wildlife trade using CITES data—Seahorses as a case study. *Aquat. Conserv. Mar. Freshw. Ecosyst.* **2016**, *26*, 154–172. [[CrossRef](#)]
25. Qin, G.; Zhang, Y.; Zhang, B.; Zhang, Y.; Liu, Y.; Lin, Q. Environmental estrogens and progestins disturb testis and brood pouch development with modifying transcriptomes in male-pregnancy lined seahorse *Hippocampus erectus*. *Sci. Total Environ.* **2020**, *715*, 136840. [[CrossRef](#)] [[PubMed](#)]
26. Tang, L.; Liu, Y.L.; Qin, G.; Lin, Q.; Zhang, Y.H. Effects of tributyltin on gonad and brood pouch development of male pregnant lined seahorse (*Hippocampus erectus*) at environmentally relevant concentrations. *J. Hazard. Mater.* **2021**, *408*, 124854. [[CrossRef](#)] [[PubMed](#)]
27. Kawaguchi, M.; Okubo, R.; Harada, A.; Miyasaka, K.; Takada, K.; Hiroi, J.; Yasumasu, S. Morphology of brood pouch formation in the pot-bellied seahorse *Hippocampus abdominalis*. *Zool. Lett.* **2017**, *3*, 19. [[CrossRef](#)]
28. Dudley, J.S.; Hannaford, P.; Dowland, S.N.; Lindsay, L.A.; Thompson, M.B.; Murphy, C.R.; Van Dyke, J.U.; Whittington, C.M. Structural changes to the brood pouch of male pregnant seahorses (*Hippocampus abdominalis*) facilitate exchange between father and embryos. *Placenta* **2021**, *114*, 115–123. [[CrossRef](#)]
29. Dudley, J.S.; Paul, J.W.; Teh, V.; Mackenzie, T.E.; Butler, T.A.; Tolosa, J.M.; Smith, R.; Foley, M.; Dowland, S.; Thompson, M.B.; et al. Seahorse brood pouch morphology and control of male parturition in *Hippocampus abdominalis*. *Placenta* **2022**, *127*, 88–94. [[CrossRef](#)]
30. Harada, A.; Shiota, R.; Okubo, R.; Yorifuji, M.; Sogabe, A.; Motomura, H.; Hiroi, J.; Yasumasu, S.; Kawaguchi, M. Brood pouch evolution in pipefish and seahorse based on histological observation. *Placenta* **2022**, *120*, 88–96. [[CrossRef](#)]
31. Whittington, C.M.; Griffith, O.W.; Qi, W.; Thompson, M.B.; Wilson, A.B. Seahorse Brood Pouch Transcriptome Reveals Common Genes Associated with Vertebrate Pregnancy. *Mol. Biol. Evol.* **2015**, *32*, 3114–3131. [[CrossRef](#)]
32. Li, C.; Li, Y.; Qin, G.; Chen, Z.; Qu, M.; Zhang, B.; Han, X.; Wang, X.; Qian, P.Y.; Lin, Q. Regulatory Role of Retinoic Acid in Male Pregnancy of the Seahorse. *Innovation* **2020**, *1*, 100052. [[CrossRef](#)]
33. Qin, G.; Luo, W.; Tan, S.; Zhang, B.; Ma, S.; Lin, Q. Dimorphism of sex and gonad-development-related genes in male and female lined seahorse, *Hippocampus erectus*, based on transcriptome analyses. *Genomics* **2019**, *111*, 260–266. [[CrossRef](#)] [[PubMed](#)]
34. Scobell, S.K.; Mackenzie, D.S. Reproductive endocrinology of *Syngnathidae*. *J. Fish. Biol.* **2011**, *78*, 1662–1680. [[CrossRef](#)]
35. Van Look, K.J.; Dzyuba, B.; Cliffe, A.; Koldewey, H.J.; Holt, W.V. Dimorphic sperm and the unlikely route to fertilisation in the yellow seahorse. *J. Exp. Biol.* **2007**, *210*, 432–437. [[CrossRef](#)] [[PubMed](#)]
36. Nickel, J.; Cursons, R. Genetic diversity and population structure of the pot-belly seahorse *Hippocampus abdominalis* in New Zealand. *N. Z. J. Mar. Freshw. Res.* **2012**, *46*, 207–218. [[CrossRef](#)]
37. Mazzoni, T.S.; Grier, H.J.; Quagio-Grassiotto, I. Germline cysts and the formation of the germinal epithelium during the female gonadal morphogenesis in *Cyprinus carpio* (Teleostei: Ostariophysi: Cypriniformes). *Anat. Rec.* **2010**, *293*, 1581–1606. [[CrossRef](#)] [[PubMed](#)]
38. Fernandez, J.A.; Bubner, E.J.; Takeuchi, Y.; Yoshizaki, G.; Wang, T.; Cummins, S.F.; Elizur, A. Primordial germ cell migration in the yellowtail kingfish (*Seriola lalandi*) and identification of stromal cell-derived factor 1. *Gen. Comp. Endocrinol.* **2015**, *213*, 16–23. [[CrossRef](#)]
39. Saito, T.; Otani, S.; Fujimoto, T.; Suzuki, T.; Nakatsuji, T.; Arai, K.; Yamaha, E. The germ line lineage in ukigori, *Gymnogobius* species (Teleostei: Gobiidae) during embryonic development. *Int. J. Dev. Biol.* **2004**, *48*, 1079–1085. [[CrossRef](#)]
40. Zhao, C.; Xu, S.; Liu, Y.; Wang, Y.; Liu, Q.; Li, J. Gonadogenesis analysis and sex differentiation in cultured turbot (*Scophthalmus maximus*). *Fish. Physiol. Biochem.* **2017**, *43*, 265–278. [[CrossRef](#)]
41. Rasmussen, T.H.; Jespersen, A.; Korsgaard, B. Gonadal morphogenesis and sex differentiation in intraovarian embryos of the viviparous fish *Zoarces viviparus* (Teleostei, Perciformes, Zoarcidae): A histological and ultrastructural study. *J. Morphol.* **2006**, *267*, 1032–1047. [[CrossRef](#)]
42. Nakamura, M.; Kobayashi, T.; Chang, X.-T.; Nagahama, Y. Gonadal sex differentiation in teleost fish. *J. Exp. Zool.* **1998**, *281*, 362–372. [[CrossRef](#)]
43. Ofelio, C.; Diaz, A.O.; Radaelli, G.; Planas, M. Histological development of the long-snouted seahorse *Hippocampus guttulatus* during ontogeny. *J. Fish. Biol.* **2018**, *93*, 72–87. [[CrossRef](#)] [[PubMed](#)]
44. Yang, Y.; Liu, Q.; Ma, D.; Xiao, Y.; Xu, S.; Wang, X.; Song, Z.; You, F.; Li, J. Spermatogonial stem cells differentiation and testicular lobules formation in a seasonal breeding teleost: The evidence from the heat-induced masculinization of genetically female Japanese flounder (*Paralichthys olivaceus*). *Theriogenology* **2018**, *120*, 68–78. [[CrossRef](#)] [[PubMed](#)]

45. Nakamura, M.; Takahashi, H. Gonadal Sex Differentiation in *Tilapia mossambica*, with Special Regard to the Time of Estrogen Treatment Effective in Inducing Complete Feminization of Genetic Males. *Bull. Fac. Fish. Hokkaido Univ.* **1973**, *24*, 1–13.
46. Mattei, C.; Mattei, X. Spermiogenesis in a teleost fish (*Lepadogaster lepadogaster*). I. The spermatid. *Biol. Cell.* **1978**, *32*, 257–266.
47. Carcupino, M.; Baldacci, A.; Corso, G.; Franzoi, P.; Pala, M.; Mazzini, M. Testis structure and symplastic spermatid formation during spermatogenesis of pipefishes. *J. Fish Biol.* **1999**, *55*, 344–353. [[CrossRef](#)]
48. Biagi, F.; Piras, F.; Farina, V.; Zedda, M.; Mura, E.; Floris, A.; Franzoi, P.; Fausto, A.M.; Taddei, A.R.; Carcupino, M. Testis structure, spermatogenesis and sperm morphology in pipefishes of the genus *Syngnathus*. *Acta Zool.* **2014**, *97*, 90–101. [[CrossRef](#)]
49. Kaur, L.; Raj, R.; Thakur, A.K.; Singh, I. Development of chitosan-catechol conjugates as mucoadhesive polymer: Assessment of acute oral toxicity in mice. *Environ. Anal. Health Toxicol.* **2020**, *35*, e2020014. [[CrossRef](#)]
50. Mazzoni, T.S.; Grier, H.J.; Quagio-Grassiotto, I. Male gonadal differentiation and the paedomorphic evolution of the testis in Teleostei. *Anat. Rec.* **2014**, *297*, 1137–1162. [[CrossRef](#)]
51. Watanabe, S.; Hara, M.; Watanabe, Y. Male Internal Fertilization and Introsperm-like Sperm of the Seaweed Pipefish (*Syngnathus schlegeli*). *Zool. Sci.* **2000**, *17*, 759–767. [[CrossRef](#)]
52. Giacomello, E.; Neat, F.C.; Rasotto, M.B. Mechanisms enabling sperm economy in blennioid fishes. *Behav. Ecol. Sociobiol.* **2007**, *62*, 671–680. [[CrossRef](#)]
53. Kvarnemo, C.; Simmons, L.W. Testes investment and spawning mode in pipefishes and seahorses (*Syngnathidae*). *Biol. J. Linn. Soc.* **2004**, *83*, 369–376. [[CrossRef](#)]

Disclaimer/Publisher’s Note: The statements, opinions and data contained in all publications are solely those of the individual author(s) and contributor(s) and not of MDPI and/or the editor(s). MDPI and/or the editor(s) disclaim responsibility for any injury to people or property resulting from any ideas, methods, instructions or products referred to in the content.